Posterodorsal medial amygdala urocortin-3, GABA and glutamate mediate suppression of LH pulsatility in female mice

Deyana Ivanova[1], Xiao-Feng Li[1], Caitlin McIntyre[1] and Kevin T O'Byrne[1]

[1]Department of Women and Children's Health, School of Life Course and Population Sciences, Faculty of Life Science and Medicine, King's College London, UK

Short title: MePD Ucn3 effect on LH and corticosterone release

Key words: Ucn3, GABA, glutamate, MePD, PVN, LH pulsatility, CORT secretion

Corresponding author's contact details: Deyana Ivanova (deyana.ivanova@kcl.ac.uk) and Kevin T O'Byrne (kevin.obyrne@kcl.ac.uk), Department of Women and Children's Health, School of Life Course and Population Sciences, Faculty of Life Science and Medicine, King's College London, 2.92W Hodgkin Building, Guy's Campus, London SE1 1UL, UK.

Reprint requests: Deyana Ivanova, Department of Women and Children's Health, School of Life Course Sciences, Faculty of Life Science and Medicine, King's College London, 2.92W Hodgkin Building, Guy's Campus, London SE1 1UL, UK.

Grants supporting paper: UKRI: BBSRC (BB/S000550/1). DI is a PhD student funded by MRC-DTP studentship.

The authors have nothing to disclose.

Abstract

The posterodorsal subnucleus of the medial amygdala (MePD) is an upstream modulator of the hypothalamic-pituitary-gonadal (HPG) and hypothalamic-pituitary-adrenal (HPA) axes. Inhibition of MePD urocortin-3 (Ucn3) neurons prevents psychological stress-induced suppression of LH pulsatility while blocking the stress-induced elevations in corticosterone (CORT) secretion in female mice. We explore the neurotransmission and neural circuitry suppressing the GnRH pulse generator by MePD Ucn3 neurons and we further investigate whether MePD Ucn3 efferent projections to the PVN control CORT secretion and LH pulsatility. Ucn3-cre-tdTomato female ovariectomised (OVX) mice were unilaterally injected with AAV-ChR2 and implanted with optofluid cannulae targeting the MePD. We optically activated Ucn3 neurons in the MePD with blue light at 10Hz and monitored the effect on LH pulses. Next, we combined optogenetic stimulation of MePD Ucn3 neurons with pharmacological antagonism of $GABA_A$ or $GABA_B$ receptors with bicuculline or CGP, respectively, as well as a combination of NMDA and AMPA receptor antagonists, AP5 and CNQX respectively, and observed the effect on pulsatile LH secretion. A separate group of Ucn3-cre-tdTomato OVX mice with oestradiol replacement were unilaterally injected with AAV-ChR2 in the MePD and implanted with fibreoptic cannulae targeting the PVN. We optically stimulated MePD Ucn3 neuron terminals with blue light at 20Hz and monitored the effect on CORT secretion and LH pulses. We reveal for the first time that activation of Ucn3 neurons in the MePD inhibits GnRH pulse generator frequency via GABA and glutamate signalling within the MePD, while MePD Ucn3 projections to the PVN modulate the HPG and HPA axes.

40 **Introduction**

41 Stress exerts a profound suppressive effect on reproduction in mammals, including rodents and
42 humans. The amygdala, part of the limbic system, is a key emotional centre integrating
43 incoming cues from the external environment, such as anxiogenic signals, with the
44 reproductive and stress axes (1). The posterodorsal sub-nucleus of the medial amygdala
45 (MePD) is an upstream modulator of pulsatile luteinizing hormone (LH) secretion (2–4) and
46 exerts an inhibitory break on pubertal timing (5,6). The MePD sends direct projections, of an
47 unknown phenotype, to the kisspeptin (kiss1) neuronal population in the hypothalamic arcuate
48 nucleus (ARC) (7,8) known as KNDy because they co-express neurokinin B (NKB) and
49 dynorphin A (Dyn) (9–11). The synchronous activity of the ARC KNDy network drives
50 pulsatile gonadotropin-releasing hormone (GnRH) and LH release (11–14). The MePD also
51 contains a kiss1 neuronal population and selective optogenetic activation of these neurons
52 increases GnRH pulse generator frequency in mice (4) and unpublished observations show this
53 is an effect involving both MePD GABA and glutamate signalling.

54 We have recently shown that urocortin-3 (Ucn3), a member of the corticotropin-releasing
55 factor (CRF) stress neuropeptide family, and its receptor CRF type 2 (CRFR2) signalling in
56 the MePD are involved in mediating the suppressive effect of psychosocial stress on LH
57 pulsatility (3). However, the underlying neural mechanisms involved in mediating the
58 inhibitory effect of MePD Ucn3 neurons on LH pulsatility remain to be established. GABA
59 and glutamate signalling in the amygdala are implicated in the modulation of anxiety behaviour
60 (15,16). The amygdala also modulates the stress response through the hypothalamic pituitary
61 adrenal (HPA) axis. The medial amygdala activates the HPA axis in response to predator odor
62 stress (17) and the MePD in particular has been shown to send stress-activated efferents to the
63 PVN (18). Furthermore, MePD Ucn3 and CRFR2 positive neurons are implicated in regulating
64 the stress response, with restraint stress increasing MePD Ucn3 (19) and social defeat elevating

65 MePD CRFR2 expression in rodents (20). Moreover, MePD Ucn3 and CRFR2 positive
66 neurons project to the PVN (21), and we have recently shown that chemogenetic inhibition of
67 MePD Ucn3 neurons prevents psychogenic stress-induced corticosterone (CORT) release in
68 female mice (3).

69 In this study, we aimed to determine whether activation of MePD Ucn3 neurons inhibits
70 pulsatile LH secretion via GABA and or glutamate signalling within this amygdala sub-
71 nucleus. To achieve this, we will combine selective optogenetic activation of MePD Ucn3
72 neurons with pharmacological antagonism of $GABA_A$ or $GABA_B$ receptors, or a combination
73 of N-methyl-D-aspartate (NMDA) and α-amino-3-hydroxy-5-methyl-4-isoxazole propionic
74 acid (AMPA) receptors, respectively, using chronically implanted intra-MePD optofluid
75 cannulae while collecting serial blood samples for LH pulse measurement in Ucn3-Cre-
76 tdTomato female mice. Additionally, we will investigate whether optogenetic stimulation of
77 MePD Ucn3 projection terminals in the PVN induce CORT release and suppress LH pulsatility.

78 **Methods**

79 **Mice**

80 Cryopreserved sperm of Ucn3-cre mice (strain Tg(Ucn3-cre)KF43Gsat/Mmucd; congenic on
81 C57BL/6 background) was acquired from MMRRC GENSAT and heterozygous transgenic
82 breeding pairs of Ucn3-Cre mice were recovered via insemination of female C57Bl6/J mice at
83 King's College London, as described previously (3). Ucn3-Cre mice were genotyped using
84 PCR for the detection of heterozygosity and Ucn3-cre mice were bred with td-Tomato mice
85 (strain B6.Cg-Gt(ROSA)26Sortm9(CAG-tdTomato)Hze/J; congenic on C57BL/6
86 background) acquired from The Jackson Laboratory, Bar Harbor, ME, USA to produce Ucn3-
87 cre-tdTomato reporter mice, as described previously (3,21). Female Ucn3-cre-tdTomato mice

88 weighing 19-23 g and aged 6-8 weeks were singly housed in individually ventilated cages
89 sealed with a HEPA-filter at 25 ± 1 °C in a 12:12 h light/dark cycle, lights on at 07:00 h
90 equipped with nesting material, wood-chip bedding and food and water ad libitum. All
91 procedures were carried out following the United Kingdom Home Office Regulations and
92 approved by the Animal Welfare and Ethical Review Body Committee at King's College
93 London.

94 **Stereotaxic injection of adeno-associated-virus carrying the channelrhodopsin construct**
95 **and fibre optic or optofluid cannula implantation**

96 All surgical procedures were carried out under aseptic conditions with general anaesthesia
97 using ketamine (Vetalar, 100 mg/kg, i.p.; Pfizer, Sandwich, UK) and xylazine (Rompun, 10
98 mg/kg, i.p.; Bayer, Leverkusen, Germany). Ucn3-Cre-tdTomato mice were secured in a David
99 Kopf stereotaxic frame (Kopf Instruments, Model 900) and either solely bilaterally
100 ovariectomised (OVX) or implanted with Silastic capsule containing 36 µg 17β-estradiol/mL
101 (E_2) in sesame oil capsule (22). These capsules produce circulating concentrations of E_2 within
102 the range observed during the diestrous phase of the estrous cycle (23,24). Estradiol is known
103 to enhance the suppressive effects of stress where the action of the gonadal steroids sensitizes
104 the HPA axis and augments stress-induced inhibition of the GnRH pulse generator in many
105 species, from rodents to primates (42–45). We had two experimental groups; OVX only and
106 OVX + E_2 capsule. The mouse brain atlas of Paxinos and Franklin (25) was used to obtain
107 target coordinates for the MePD (2.30 mm lateral, -1.55 mm from bregma, at a depth of -4.94
108 mm below the skull surface). To reveal the skull an incision was made of the scalp and one
109 small hole was drilled above the location of the right MePD. AAV9-EF1a-double floxed-
110 hChR2(H134R)-EYFP-WPRE-HGHpA (300 nL; $3x10^{11}$ GC/ml; Serotype:9; Addgene,
111 Massachusetts, USA) was unilaterally injected into the right MePD using a 2-µL Hamilton

112 micro syringe (Esslab, Essex, UK) over 10 min, using the robot stereotaxic system (Neurostar,
113 Tubingen, Germany), performed for the targeted expression of ChR2-EYFP in MePD Ucn3
114 neurons. After injection, the needle was left in position for a further 5 min and lifted slowly
115 over 2 min. Cre-positive mice received the AAV-ChR2 injection (test mice) or a control virus
116 AAV-YFP (Addgene) (control mice). The control virus does not contain the ChR2 construct.
117 The mice were then implanted with a dual optofluid cannula (Doric Lenses, Quebec, Canada)
118 at the same AP and ML coordinates as the viral injection site, however a different DV was used
119 such that the internal cannula targets the MePD and the fibre optic cannula is situated 0.2 mm
120 above the MePD site. Once in position the optofluid cannula was secured on the skull using
121 dental cement (Super-Bond Universal Kit, Prestige Dental, UK) and the incision of the skin
122 was closed with suture. Mice were left to recover for one week and after recovery period, mice
123 were handled daily to acclimatise to experimental procedures for a further 2 weeks. Thirteen
124 mice received the AAV-ChR2 injection and were implanted with an optofluid cannula in the
125 MePD. Five mice received the control AAV-YFP and were implanted with an optofluid
126 cannula in the MePD. Eleven mice received the AAV-ChR2 injection in the MePD and were
127 implanted with an optic fibre in the PVN. Five mice received the control AAV-YFP and were
128 implanted with an optic fibre in the PVN.

129 **In vivo optogenetic stimulation of MePD Urocortin-3 neurons**

130 In order to test the effect of optogenetic stimulation of MePD Ucn3 neurons on LH pulsatility
131 the ferrule of the implanted optofluid cannula, on the right side of the MePD, was attached via
132 a ceramic mating sleeve to a multimode fibre optic rotatory joint patch cable (Thorlabs LTD,
133 Ely, UK) at a length allowing for free movement of the mouse in their cage and blue light (473
134 nm wavelength; 10 mW) was delivered using a Grass SD9B stimulator-controlled laser
135 (Laserglow Technologies, Toronto, Canada). The mice were left to acclimatise for 1 h.

136 Following the acclimatisation period blood samples (5 µL) were collected every 5 min for 2 h
137 where after 1 h of control blood sampling, Ucn3-cre-tdTomato mice received optic stimulation
138 at 10 Hz with a 10 ms pulse interval and pattern stimulation of 5 seconds on and 5 seconds off
139 for the remaining 1 h.

140 **Intra-MePD administration of bicuculline (BIC), CGP-35348 or AP5 + CNQX during**
141 **optogenetic stimulation of MePD Urocortin-3 neurons**

142 Neuropharmacological manipulation of GABA and glutamate receptor signalling in the MePD
143 with or without optogenetic stimulation of MePD Ucn3 neurons was done to test whether
144 MePD Ucn3 induced suppression of LH pulsatility involves GABA or glutamate receptor
145 signalling. OVX mice implanted with a optofluid cannula in the MePD were subjected to the
146 tail-tip blood collection procedure, as previously described (26). Infusion of drugs with or
147 without optogenetic stimulation and blood sampling were performed between 09:00-13:00 h,
148 where 5 µl blood was collected every 5 min for 2 h. Internal cannula (Doric Lenses) attached
149 to extension tubing (0.58 mm ID, 0.96 mm OD), preloaded with bicuculline (BIC) ($GABA_A$
150 receptor antagonist; Sigma-Aldrich), CGP-35348 ($GABA_B$ receptor antagonist; Sigma-
151 Aldrich), AP5 + CNQX cocktail (NMDA and AMPA receptor antagonists; Tocris) or aCSF as
152 vehicle control, was inserted into the guide cannula of the optofluid implant and mice were
153 connected to the laser as described above. The tubing for drug infusion extended beyond the
154 cage and the distal ends were attached to 10-µl Hamilton syringes (Waters Ltd, Elstress, UK)
155 fitted into a PHD 2000 Programmable syringe pump (Harvard Apparatus, Massachusetts,
156 USA), allowing for a continuous infusion of the drug at a constant rate and mice were kept in
157 the cage throughout the experiment, freely-moving with food and water *ad libitum*. After 55
158 min of control blood sampling, the mice were given an initial bolus injection, 0.30 µl at a rate
159 of 0.06 µl/min over 5 min, of BIC, CGP-35348, AP5 + CNQX or aCSF. The laser was turned

160 on at 60 min and the bolus injection was followed by a continuous infusion, 0.8 µl at a rate of
161 0.01 µl/min over 1 h, of BIC, CGP-35348, AP5 + CNQX or aCSF. BIC, CGP-35348, AP5 and
162 CNQX were dissolved in aCSF to reach bolus concentrations of 20 pmol, 4.5 nmol, 1.2 nmol
163 and 0.5 nmol respectively. The concentrations for the continuous infusion of BIC, CGP-35348,
164 AP5 and CNQX were 68 pmol, 15 nmol, 2nmol and 1 nmol respectively. In the absence of
165 optic stimulation, the same regimen was applied. The mice receive all treatments in a random
166 order, with at least 2 days between experiments.

167 **MePD Urocortin-3 terminal optogenetic stimulation in the PVN**

168 To test the effect of optogenetic stimulation of MePD Ucn3 neuronal terminals in the PVN on
169 LH pulsatility and CORT release, OVX + E_2 Ucn3-cre-tdTomato mice with AAV-ChR2
170 injection in the right MePD implanted with a fibre optic cannula in the right PVN were
171 subjected to the tail-tip blood collection procedure, as previously described (26). For LH
172 measurement, blood samples were collected every 5 min for 2 h, as described above. Mice
173 were connected to the laser as described above. Optogenetic stimulation was initiated after the
174 1 h control blood sampling period and Ucn3-cre-tdTomato mice received optic stimulation at
175 20 Hz, 15 mW with a 10 ms pulse interval and pattern stimulation of 5 seconds on and 5
176 seconds off for the remaining 1 h. For CORT measurements, 15 µl blood samples were
177 collected on a separate occasion and blood samples were stored in tubes containing 5 µl
178 heparinised saline (5 IU ml^{-1}). Optogenetic stimulation was initiated, as described above, 30
179 min into the experiment (time point, 0 min) and lasted for 1 h (time point 60 min). Remaining
180 blood samples were collected at 0, 30 and 60 min, with a final sample taken 1 h after the
181 termination of optogenetic stimulation (time point, 120 min). At the end of the experiment,
182 blood samples were centrifuged at 13,000 RPM for 20 min at 20°C and plasma stored at -20°C.
183 All experiments were performed between 9:00-12:00 h.

184 **Validation of AAV injection and cannula implant site**

185 Upon completion of experiments, mice were anaesthetised with a lethal dose of ketamine and
186 transcardial perfusion was performed with heparinised saline for 5 min followed by ice-cold
187 4% paraformaldehyde (PFA) in phosphate buffer (pH 7.4) for 15 min using a pump (Minipuls,
188 Gilson, Villiers Le Bel, France). Mice brains were collected immediately and post-fixed in
189 15% sucrose in 4% PFA at 4 °C and left to sink. Once sunk, they were transferred to 30%
190 sucrose in phosphate-buffered saline (PBS) and left to sink. Brains were snap-frozen in
191 isopropanol on dry ice and stored in -80°C until further processing. Every third coronal brain
192 section (30-µm/section) through-out the MePD region (-1.34 mm to -2.70 mm from bregma)
193 was collected using a cryostat (Bright Instrument Co., Luton, UK). Sections were mounted on
194 microscope slides, air dried and covered with ProLong Antifade mounting medium (Molecular
195 Probes, Inc. OR, USA). Cannula placement and AAV injection site was verified with
196 Axioskop 2 Plus microscope equipped with Axiovision, version 4.7 (Zeiss) by determining
197 whether cannula reach the MePD. For AAV-ChR2-EYFP injected Ucn3-cre-tdTomato mice
198 we determined whether MePD Ucn3 neurons were infected by merging td-Tomato
199 fluorescence of Ucn3 neurons with YFP fluorescence in the MePD, as described previously
200 (3). Axioskop 2 Plus microscope (Carl Zeiss) equipped with axiovision, version 4.7 (Carl
201 Zeiss) was used to take images. Only mice with correct AAV injection and cannula placement
202 in the MePD were analysed.

203 **LH and CORT measurement**

204 Mice were handled daily to acclimatise to the tail-tip blood sampling procedure for LH
205 measurement (3). Blood samples collected for LH measurement were processed using LH
206 ELISA, as previously reported (3). The capture antibody (monoclonal antibody, anti-bovine
207 LHβ subunit, AB_2665514) was purchased from Department of Animal Science at the

208 University of California, Davis. The mouse LH standard (AFP-5306A) and primary antibody
209 (polyclonal antibody, rabbit LH antiserum, AB_2665533) were obtained from Harbour-UCLA
210 (California, USA). The secondary antibody (Horseradish-Peroxidase (HRP)-linked donkey
211 anti-rabbit IgG polyclonal antibody, AB_772206) was purchased from VWR International
212 (Leicestershire, UK). Intra-assay and inter-assay variations were 4.6% and 10.2%, respectively
213 and the assay sensitivity was 0.0015 ng/mL. DynPeak algorithm was used for the detection of
214 LH pulses (3). The effect of optogenetic stimulation of MePD Ucn3 neurons and
215 neuropharmacology studies was established by comparing the LH inter-pulse interval (IPI)
216 from the 1 h control period (pre-stimulation) or drug administration control period to the 1 h
217 experimental period, as previously described (3).

218 Blood samples were collected for CORT measurement were processed using a commercially
219 available enzyme immunoassay (EIA) kit (sheep polyclonal antibody specific for
220 corticosterone, AB_2877626; DetectX® Corticosterone Enzyme Immunoassay Kit, K014;
221 Arbor Assays, Michigan, USA), as described previously (3).

222 **Statistics**

223 Mice were compared between groups using a one-way ANOVA with a Tukey post-hoc and
224 data was presented as mean ± SEM. Statistics were performed using Igor Pro 7, Wavemetrics,
225 Lake Oswego, OR, USA. Data was represented as mean ± SEM and +$p<0.05$, ++$p<0.001$ and
226 +++$p<0.0001$ were considered to be significant.

227 **Results**

228 **Effects of optogenetic stimulation of MePD Urocortin-3 neurons on LH pulse frequency**

229 Optogenetic stimulation of MePD Ucn3 neurons in control mice had no effect on LH pulse
230 interval (Fig. 1A; AAV-YFP: n = 3) and administration of aCSF alone (AAV-YFP with no

231 stimulation: n = 2) had no effect on LH pulse interval. Optogenetic stimulation of MePD Ucn3
232 neurons with blue light at 10 Hz, 10 mW suppressed pulsatile LH secretion (Fig. 1B; AAV-
233 ChR2: n = 9). These data are summarized in the figure 1C.

234 **Effects of intra-MePD administration of bicuculline (BIC), a $GABA_AR$ antagonist, and**
235 **CGP, a $GABA_BR$ antagonist, during optical stimulation of MePD Urocortin-3 neurons**
236 **on LH pulsatility**

237 Delivery of BIC alone had no significant effect on LH pulsatility (Fig. 1D; n = 8). Intra-MePD
238 infusion of BIC during optogenetic stimulation of MePD Ucn3 neurons with blue light at 10
239 Hz, 10 mW completely blocked the suppressive effect of MePD Ucn3 neuronal activation on
240 LH pulsatility (Fig. 1E; n = 9). The results of this experiment are summarised in the figure 1F.

241 **Effects of intra-MePD administration of CGP, a $GABA_BR$ antagonist, during optical**
242 **stimulation of MePD Urocortin-3 neurons on LH pulsatility**

243 Delivery of CGP alone had no significant effect on LH pulsatility (Fig. 1G; n = 7). Intra-MePD
244 infusion of CGP during optogenetic stimulation of MePD Ucn3 neurons with blue light at 10
245 Hz, 10 mW completely blocked the suppressive effect of MePD Ucn3 neuronal activation on
246 LH pulsatility (Fig. 1H; n = 7). The results of this experiment are summarised in the figure 1I.

247 **Effects of intra-MePD glutamate antagonism during optogenetic stimulation of MePD**
248 **Urocortin-3 neurons on LH pulsatility**

249 Delivery of AP5 + CNQX alone had no significant effect on LH pulsatility (Fig. 1J; n = 6).
250 Intra-MePD infusion of AP5 (selective NMDA antagonist) + CNQX (selective AMPA
251 antagonist) during optogenetic stimulation of MePD Ucn3 neurons with blue light at 10 Hz, 10
252 mW completely blocked the suppressive effect of MePD Ucn3 neuronal activation on LH
253 pulsatility (Fig. 1K; n = 6). The results of this experiment are summarised in the figure 1L.

254 **Effect of MePD Urocortin-3 terminal stimulation in the PVN on dynamic CORT secretion**

255 Optogenetic stimulation of MePD Ucn3 neuron terminals in the PVN with blue light at 20 Hz,
256 15 mW elevated CORT secretion compared to controls (Fig. 2; AAV-ChR2: n = 6).
257 Optogenetic stimulation of MePD Ucn3 neurons and terminal projections in the PVN in control
258 mice had no effect on dynamic CORT secretion (AAV-YFP; n = 4).

259 **Effect of MePD Urocortin-3 terminal stimulation in the PVN on LH pulsatility**

260 Optogenetic stimulation of MePD Ucn3 projections in the PVN in control mice had no effect
261 on LH pulse interval (Fig. 3A; AAV-YFP, n = 3; wild-type with AAV-ChR2, n = 2) and no
262 stimulation of the MePD Ucn3 projections in the PVN (no stimulation, n = 2) had no effect on
263 LH pulse interval. Optogenetic stimulation of MePD Ucn3 neuron terminals in the PVN with
264 blue light at 20 Hz, 15 mW reduced LH pulsatility compared to controls (Fig. 3B; AAV-ChR2:
265 n = 8). The results of this experiment are summarised in the figure 3C.

266 **Selective expression of ChR2 in MePD Ucn3 neurons and MePD Ucn3 neuron**
267 **projections in the PVN, and validation of cannula position**

268 Evaluation of AAV9-EF1a-double floxed-hChR2(H134R)-EYFP-WPRE-HGHpA expression
269 in tdTomato labelled neurons from AAV-injected Ucn3-cre-tdTomato mice revealed that 87.00
270 ± 6.00% of MePD Ucn3 neurons expressed AAV-ChR2 and the number of tdTomato labelled
271 Ucn3 neurons per side per slice in the MePD was counted at 49.00 ± 5.37 (mean ± SEM) with
272 the number of AAV-hM4D-mCitrine infected neurons being 43.01 ± 3.65 (mean ± SEM)
273 (n=8). A representative example is shown in Fig 4, A-C. The optofluid cannula was also
274 verified to be correctly positioned in the MePD in all of 8 mice. Evaluation of AAV9-EF1a-
275 double floxed-hChR2(H134R)-EYFP-WPRE-HGHpA expression in Ucn3 projections from
276 the MePD to the PVN showed YFP labelled fibres in the PVN Fig 5, A-Aii. Local Ucn3

277 neurons in the PVN are labelled with tdTomato. The optic fibre cannula was also verified to
278 be correctly positioned in the PVN in all of 8 mice (Fig. 5A).

279 **Discussion**

280 We show optogenetic stimulation of MePD Ucn3 neurons inhibits pulsatile LH secretion, an
281 effect that was completely blocked by intra-MePD GABA and glutamate antagonism.
282 Moreover, optogenetic stimulation of MePD Ucn3 projections in the hypothalamic PVN also
283 suppresses LH pulsatility while inducing release of CORT. These results demonstrate that
284 inhibition of the GnRH pulse generator by Ucn3 neurons within the MePD relies on GABA
285 and glutamate signalling in the MePD, *per se*. Moreover, MePD Ucn3 efferent projections in
286 the PVN modulate the activity of the HPA and HPG axes.

287 The MePD is a major upstream regulator of gonadotropic hormone secretion with a significant
288 population of GABAergic neurons projecting to reproductive neural centres in the
289 hypothalamus (27). Although classic lesioning studies suggest an inhibitory output of the
290 MePD over reproductive function (28,29), selective optical stimulation of MePD kiss1 neurons
291 increases LH pulse frequency (4), which our unpublished observations show relies upon both
292 GABA and glutamate signalling in the MePD. Due to this interesting dichotomy, we have
293 proposed a disinhibitory system, which is consistent with the pallidal origin of this limbic
294 structure (30), whereby MePD kiss1 activation excites inhibitory GABAergic interneurons,
295 which in turn reduces the inhibitory tone of the GABAergic projections from the MePD to the
296 ARC KNDy network allowing for an increase in GnRH pulse generator frequency (4).
297 Contrastingly, kisspeptin antagonism, reducing MePD kiss1 signalling decreases GnRH pulse
298 generator frequency (31).

299 We have recently shown that stress-induced activation of Ucn3 and CRFR2 signalling within
300 the MePD inhibits GnRH pulse generator activity (3) and activation of MePD Ucn3 neurons

301 delays pubertal timing (32). It has also been shown that the majority of MePD CRFR2
302 expressing neurons are GABAergic (21). In the MePD, Ucn3 fibres overlap with sites
303 expressing its cognate receptor CRFR2 (33,34) and some local Ucn3 neurons within the MePD
304 are shown to have an interneuron-like appearance (35), thus Ucn3 neurons may form
305 connections with and signal via GABAergic CRFR2 positive neurons in this region. In the
306 present study, we show that optogenetic activation of MePD Ucn3 neurons inhibits pulsatile
307 LH secretion. Therefore, we propose that activated MePD Ucn3 neurons may signal through
308 inhibitory GABAergic CRFR2 interneurons, upstream to the MePD kiss1 neurons,
309 downregulating MePD kiss1 signalling resulting in decreased GnRH pulse generator
310 frequency.

311 In our proposed model, we hypothesised that GABA signalling is an important factor mediating
312 the suppressive effect of MePD Ucn3 activation on GnRH pulse generator activity. Therefore,
313 we tested the effect of intra-MePD administration of $GABA_A$ or $GABA_B$ receptor antagonists
314 during optical stimulation of MePD Ucn3 neurons on LH pulsatility, and indeed, we found that
315 both $GABA_A$ and $GABA_B$ receptor antagonism blocks the suppression of LH pulses by MePD
316 Ucn3 neuronal activation. From our previous studies, we know MePD Ucn3 neurons mediate
317 psychosocial stress-induced inhibition of LH pulsatility (3). Based on our proposed neuronal
318 circuit, $GABA_A$ and $GABA_B$ receptor antagonism may be working upstream and downstream
319 of MePD kiss1 activity to cancel both the inhibitory GABAergic CRFR2 interneurons upstream
320 to and the inhibitory GABAergic interneurons downstream to MePD kiss1 neurons. Therefore,
321 the inhibitory output of the MePD GABAergic projection neurons to the ARC KNDy network
322 is cancelled, thus, negating the suppressive effect of MePD Ucn3 activation on the GnRH pulse
323 generator. Essentially, terminating the ability of the GABA interneuron, upstream and
324 downstream of MePD kiss1 activity, to take part in the disinhibition by antagonising GABA

325 receptors on the MePD kiss1 neurons as well as post-synaptic GABA projection neurons
326 removing the inhibitory control over the GnRH pulse generator from the MePD.

327 We have identified GABA signalling as a key part of the MePD Ucn3 neural circuitry
328 associated with suppression of the GnRH pulse generator, however glutamate signalling in the
329 amygdala is also known to be involved in modulating reproduction and anxiety-behaviour (36).
330 Administration of NMDA into the MePD disrupts ovarian cycles in rats, while NMDA receptor
331 antagonism in the MePD delays pubertal timing (29). Urocortins can function endogenously
332 as modulators of excitatory glutamatergic transmission in the amygdala, with *in vitro* studies
333 showing modulation of glutamatergic excitatory post-synaptic potentials via pre- and
334 postsynaptic CRFR2-mediated mechanisms (37). Moreover, Ucn3 neurons may be
335 glutamatergic, as shown in the hypothalamic perifornical area, where they are activated during
336 infant-directed aggression (38) and increase anxiety-like behaviour (39), but this awaits future
337 study for the MePD Ucn3 population. Therefore, we hypothesised that glutamate
338 neurotransmission may form a critical part of the MePD Ucn3 neural circuitry involved in
339 stress-induced inhibition of GnRH pulse generator activity. In the present study, we show that
340 intra-MePD AMPA and NMDA receptor antagonism blocks the inhibitory effect of MePD
341 Ucn3 neuronal activation on LH pulsatility. These observations suggest the involvement of
342 similar neural circuitry as in the neighbouring posteroventral medial amygdala which exhibits
343 functional glutamatergic signalling onto inhibitory GABA neurons (30). Moreover, inhibition
344 of both GABA and glutamate signalling is equally effective at blocking suppression of LH
345 pulses suggesting they are key components in the circuit. Building upon our proposed neuronal
346 circuit, MePD Ucn3 expressing neurons may be glutamatergic modulating excitatory post-
347 synaptic signals to activate inhibitory GABAergic CRFR2 positive interneurons, which in turn
348 downregulate MePD kiss1 activity, resulting in suppression of GnRH pulse generator activity.
349 Thus, NMDAR and AMPAR antagonism possibly cancels MePD Ucn3 glutamatergic

350 activation of inhibitory GABAergic CRFR2 inter-neurons preventing the decrease in GnRH
351 pulse generator activity.

352 Stress elevates Ucn3 mRNA (19) and c-fos expression in the MePD (18) while chemogenetic
353 inhibition of MePD Ucn3 neurons prevents stress-induced suppression of LH pulsatility (3).
354 The MePD sends stress-activated efferents to the PVN (18) and more recently MePD Ucn3
355 neurons have been shown to project directly to the PVN (21). In the current study, we
356 demonstrate for the first time that optical stimulation of MePD Ucn3 projections in the PVN
357 inhibits pulsatile LH secretion. Moreover, chemogenetic activation of PVN CRF neuron
358 perikarya rapidly suppresses LH pulse frequency, however optogenetic activation of their nerve
359 terminals in the ARC does not affect the firing of KNDy neurons (40) and directly injecting
360 CRF in the ARC also has no effect on LH secretion (41), suggesting the involvement of an
361 indirect mechanism modulating GnRH pulse generator activity. Since MePD Ucn3 neurons
362 receive inputs from the PVN (21) and the MePD sends direct efferent projections to KNDy
363 neurons of an unknown neurochemical phenotype (8), this amygdala structure may function as
364 a relay centre between the PVN and ARC, to regulate stress signals to the GnRH pulse
365 generator as well as contributing to cross talk between the HPA and HPG axes.

366 Central administration of Ucn3 augments the HPA axis response to restraint stress in rats (19)
367 and increases hypothalamic CRF concentrations and circulating levels of CORT in mice (42).
368 Overexpression of Ucn3 in the hypothalamic perifornical area increases anxiety-like behaviour
369 (39) and activation of the CRFR2 in the lateral septum is involved in stress-induced persistent
370 anxiety in mice (43). In the medial amygdala, Ucn3 neuronal populations are shown to consist
371 of both projection neurons extending to the PVN, the bed nucleus of the stria terminalis and
372 the suprachiasmatic nucleus (21,35) and local interneurons where Ucn3 neuronal fibres overlap
373 with CRFR2-expression (33,34). We have previously shown chemogenetic inhibition
374 targeting both local and efferent MePD Ucn3 neurons prevents psychosocial stress-induced

375 release of CORT (3). In the present study, we show that selective optogenetic activation of
376 MePD Ucn3 projections in the PVN elevates CORT secretion, thus MePD Ucn3 projections to
377 the PVN are critical for the regulation of CORT secretion. Further work is required to identify
378 whether only the MePD Ucn3 projecting efferents to the PVN are crucial for regulating CORT
379 secretion. The presence of estradiol is known to up-regulate basal CRF mRNA levels in the
380 PVN in rodents and induce high levels of circulating corticosterone providing a sensitizing
381 effect to the activity of the HPA axis (44,45). Therefore, we implanted the OVX mice with
382 estradiol capsules producing circulating concentrations of estradiol within the range observed
383 during the diestrous phase of the estrous cycle for HPA axis sensitization in mice similarly to
384 what has been reported in previous studies (23,24,46). PVN-CRF neurons express mRNA
385 transcripts for CRFR2 (47) and CRFR2 primarily activate the Gαs adenylyl cyclase/cAMP
386 signalling pathway (48) indicating that signalling via the CRFR2 located on PVN-CRF neurons
387 may result in activation of this neuronal population and hence the HPA axis. Therefore, Ucn3
388 released following optical stimulation of MePD Ucn3 projections in the PVN may directly
389 activate the PVN-CRF neurons, signalling via CRFR2, to stimulate CORT release.

390 Selective CRFR2 antagonism has been shown to reverse the stress-induced inhibition of LH
391 pulses (49) where central administration of astressin2-B, a specific CRFR2 antagonist, blocked
392 the restraint-stress induced suppression of pulsatile LH secretion in rats (50). We have shown
393 specific antagonism of CRFR2 in the MePD blocked the inhibitory effects of predator odor on
394 the GnRH pulse generator in mice (3) and activation of MePD Ucn3 neurons delayed puberty
395 in mice (32). Therefore, we know CRFR2 neurons are involved in processing stressful
396 information and coordinating the activity of the GnRH pulse generator accordingly.
397 Additionally, CRF is also implicated in reducing pulsatile LH secretion via CRFR1 expressing
398 neurons in mice (51). Chronic stress levels of CORT decrease LH pulsatility (46) and recently
399 an acute rise in CORT sustained for 30-60 min was shown to inhibit pulsatile LH release, but

400 only in OVX mice with estrogen replacement (52) and after a delay of approximately 30 min
401 following the CORT rise. From our observations, inhibition of LH pulsatility occurs
402 immediately after the stimulation of MePD Ucn3 projections in the PVN in OVX estradiol
403 replaced mice, thus it is unlikely the result of negative feedback from CORT release but rather
404 a central suppression of GnRH pulse generator activity possibly from the activation of PVN
405 CRF neurons, although the mechanism involved has yet to be established. The PVN CRF
406 neuronal population was not traditionally considered important for mediating stress-induced
407 suppression of pulsatile LH secretion, as PVN lesion studies have shown that this region is not
408 critical in mediating the stress-induced suppression of the reproductive axis (53). However,
409 with the recent observations showing that chemogenetic activation of PVN CRF neurons
410 indirectly inhibits the GnRH pulse generator it is plausible that the stress neural circuitry
411 includes upstream signalling via the MePD. Therefore, a possible route may involve stressful
412 information processed by the PVN CRF neurons relayed via the MePD Ucn3 neuronal circuitry
413 to the ARC KNDy neurons to modulate their activity. The neighbouring central nucleus of the
414 amygdala is known to act as a relay centre in pain control where the central lateral part receives
415 nociceptive input from the parabrachial nucleus and the central medial part is involved in
416 regulating the output of defensive behaviour and nociception (54). Local and efferent MePD
417 Ucn3 signalling plays a critical dual role in regulating GnRH pulse generator activity and
418 CORT secretion, thus MePD Ucn3 neuronal populations and their projections may represent a
419 nodal centre in the interaction between the reproductive and stress axes.

420 Our findings show for the first time that stimulation of local Ucn3 neurons in the MePD inhibits
421 GnRH pulse generator activity involving an interplay between Ucn3, GABA and glutamate
422 signalling within the MePD. Furthermore, we interrogate the MePD Ucn3 neuron projection
423 terminals in the PVN demonstrating that stimulation of the MePD Ucn3 efferent projections in
424 the PVN elevates CORT secretion to stress levels while suppressing the GnRH pulse generator.

425 How the local neural circuit within the MePD engages with efferent projections from the MePD
426 to the PVN and the interplay between Ucn3, GABA and glutamate neurons to mediate the
427 suppressive effect on LH pulsatility and the stimulatory effect on the HPA axis remains an
428 exciting question for the future.

429 **Bibliography**

430 1. Ressler KJ. Amygdala Activity, Fear, and Anxiety: Modulation by Stress. Biol
431 Psychiatry. 2010;67(12):1117–9.

432 2. Lin Y, Li XF, Lupi M, Kinsey-Jones JS, Shao B, Lightman SL, O'Byrne KT . The role
433 of the medial and central amygdala in stress-induced suppression of pulsatile LH
434 secretion in female rats. Endocrinology. 2011;152(2):545–55.

435 3. Ivanova D, Li XF, McIntyre C, Liu Y, Kong L, O'Byrne KT . Urocortin3 in the
436 Posterodorsal Medial Amygdala Mediates Stress-induced Suppression of LH
437 Pulsatility in Female Mice. Endocrinology. 2021;162(12):bqab206.

438 4. Lass G, Li XF, de Burgh RA, He W, Kang Y, Hwa-Yeo S, Sinnett-Smith LC,
439 Manchishi SM, Colledge WH, Lightman SL, O'Byrne KT . Optogenetic stimulation of
440 kisspeptin neurones within the posterodorsal medial amygdala increases luteinising
441 hormone pulse frequency in female mice. J Neuroendocrinol. 2020;32(2):e12823.

442 5. Li XF, Adekunbi DA, Alobaid HM, Li S, Pilot M, Lightman SL, O'Byrne KT . Role
443 of the posterodorsal medial amygdala in predator odour stress-induced puberty delay
444 in female rats. J Neuroendocrinol. 2019;31(6):e12719.

445 6. Adekunbi DA, Li XF, Li S, Adegoke OA, Iranloye BO, Morakinyo AO, Lightman SL,
446 Taylor PD, Poston L, O'Byrne KT . Role of amygdala kisspeptin in pubertal timing in
447 female rats. PLoS One. 2017;12(8):e0183596.

448 7. Moore AM, Coolen LM, Lehman MN. Kisspeptin/Neurokinin B/Dynorphin (KNDy)
449 cells as integrators of diverse internal and external cues: evidence from viral-based
450 monosynaptic tract-tracing in mice. Sci Rep. 2019;9(1):1–5.

451 8. Yeo SH, Kyle V, Blouet C, Jones S, Colledge WH. Mapping neuronal inputs to Kiss1
452 neurons in the arcuate nucleus of the mouse. PLoS One. 2019;14(3):e0213927.

453 9. Qiu J, Nestor CC, Zhang C, Padilla SL, Palmiter RD, Kelly MJ, Rønnekleiv OK .
454 High-frequency stimulation-induced peptide release synchronizes arcuate kisspeptin
455 neurons and excites GnRH neurons. Elife. 2016;5:e16246.

456 10. Clarkson J, Han SY, Piet R, McLennan T, Kane GM, Ng J, Porteous RW, Kim JS,
457 Colledge WH, Iremonger KJ HA. Definition of the hypothalamic GnRH pulse
458 generator in mice. Proc Natl Acad Sci U S A. 2017;114(47):e10216–23.

459 11. Voliotis M, Li XF, De Burgh R, Lass G, Lightman SL, O'Byrne KT, Tsaneva-
460 Atanasova K . The Origin of GnRH pulse generation: An integrative mathematical-
461 experimental approach. J Neurosci. 2019;39(49):9738–47.

462 12. Moore AM, Coolen LM, Lehman MN. In vivo imaging of the GnRH pulse generator
463 reveals a temporal order of neuronal activation and synchronization during each pulse.
464 Proc Natl Acad Sci U S A. 2022;119(6).

465 13. Han SY, McLennan T, Czieselsky K, Herbison AE. Selective optogenetic activation of
466 arcuate kisspeptin neurons generates pulsatile luteinizing hormone secretion. Proc Natl
467 Acad Sci U S A. 2015;112(42):13109–14.

468 14. Voliotis M, Li XF, De Burgh RA, Lass G, Ivanova D, McIntyre C, O'Byrne K,
469 Tsaneva-Atanasova K . Modulation of pulsatile GnRH dynamics across the ovarian
470 cycle via changes in the network excitability and basal activity of the arcuate
471 kisspeptin network. Elife. 2021;10.

472 15. Martin EI, Ressler KJ, Binder E, Nemeroff CB. The Neurobiology of Anxiety
473 Disorders: Brain Imaging, Genetics, and Psychoneuroendocrinology. Psychiatr Clin
474 North Am. 2009;32(3):549.

475 16. Nuss P. Anxiety disorders and GABA neurotransmission: A disturbance of
476 modulation. Neuropsychiatr Dis Treat. 2015;11:165–75.

477 17. Takahashi LK. Olfactory systems and neural circuits that modulate predator odor fear.
478 Front Behav Neurosci. 2014;8:72.

479 18. Van-Hover C, Li C. Stress-activated afferent inputs into the anterior parvicellular part
480 of the paraventricular nucleus of the hypothalamus: Insights into urocortin 3 neuron
481 activation. Brain Res. 2015;1611:29–43.

482 19. Jamieson PM, Li C, Kukura C, Vaughan J, Vale W. Urocortin 3 modulates the
483 neuroendocrine stress response and is regulated in rat amygdala and hypothalamus by
484 stress and glucocorticoids. Endocrinology. 2006;147(10):4578–88.

485 20. Fekete ÉM, Zhao Y, Li C, Sabino V, Vale WW, Zorrilla EP. Social defeat stress
486 activates medial amygdala cells that express type 2 corticotropin-releasing factor
487 receptor mRNA. Neuroscience. 2009;162(1):5–13.

488 21. Shemesh Y, Forkosh O, Mahn M, Anpilov S, Sztainberg Y, Manashirov S,
489 Shlapobersky T, Elliott E, Tabouy L, Ezra G, Adler ES . Ucn3 and CRF-R2 in the
490 medial amygdala regulate complex social dynamics. Nat Neurosci. 2016;19(11):1489–
491 96.

492 22. Ström JO, Theodorsson A, Ingberg E, Isaksson IM, Theodorsson E. Ovariectomy and
493 17β-estradiol Replacement in Rats and Mice: A Visual Demonstration. J Vis Exp.
494 2012;(64):4013.

495 23. Phumsatitpong C, Moenter SM. Estradiol-Dependent stimulation and suppression of

496 gonadotropin-Releasing hormone neuron firing activity by corticotropin-Releasing
497 hormone in female mice. Endocrinology. 2018;159(1):414–25.

498 24. Czieselsky K, Prescott M, Porteous R, Campos P, Clarkson J, Steyn FJ, Campbell RE,
499 Herbison AE . Pulse and Surge Profiles of Luteinizing Hormone Secretion in the
500 Mouse. Endocrinology. 2016;157(12):4794–802.

501 25. Paxinos G, Franklin KB . Mouse Brain in Stereotaxic Coordinates. Acad Press.
502 2019;5:246.

503 26. McCosh RB, Kreisman MJ, Breen KM. Frequent tail-tip blood sampling in mice for
504 the assessment of pulsatile luteinizing hormone secretion. J Vis Exp. 2018;(137).

505 27. Pardo-Bellver C, Cádiz-Moretti B, Novejarque A, Martínez-García F, Lanuza E.
506 Differential efferent projections of the anterior, posteroventral, and posterodorsal
507 subdivisions of the medial amygdala in mice. Front Neuroanat. 2012;6(33):1–26.

508 28. Stephens SBZ, Raper J, Bachevalier J, Wallen K. Neonatal amygdala lesions advance
509 pubertal timing in female rhesus macaques. Psychoneuroendocrinology. 2015;51:307–
510 17.

511 29. Li XF, Hu MH, Hanley BP, Lin YS, Poston L, Lightman SL, O'Byrne KT . The
512 posterodorsal medial amygdala regulates the timing of puberty onset in female rats.
513 Endocrinology. 2015;156(10):3725–36.

514 30. Keshavarzi S, Sullivan RKP, Ianno DJ, Sah P. Functional properties and projections of
515 neurons in the medial amygdala. J Neurosci. 2014;34(26):8699–715.

516 31. Comninos AN, Anastasovska J, Sahuri-Arisoylu M, Li XF, Li S, Hu M, Jayasena CN,
517 Ghatei MA, Bloom SR, Matthews PM, O'Byrne KT . Kisspeptin signaling in the
518 amygdala modulates reproductive hormone secretion. Brain Struct Funct.
519 2016;221(4):2035–47.

520 32. Ivanova D, Li X, Liu Y, McIntyre C, Fernandes C, Lass G, Kong L, O'Byrne KT .
521 Role of Posterodorsal Medial Amygdala Urocortin-3 in Pubertal Timing in Female
522 Mice. Front Endocrinol (Lausanne). 2022;0:910.

523 33. Cavalcante JC, Sita LV, Mascaro MB, Bittencourt JC, Elias CF. Distribution of
524 urocortin 3 neurons innervating the ventral premammillary nucleus in the rat brain.
525 Brain Res. 2006;1089(1):116–25.

526 34. Li C, Vaughan J, Sawchenko PE, Vale WW. Urocortin III-immunoreactive projections
527 in rat brain: Partial overlap with sites of type 2 corticotrophin-releasing factor receptor
528 expression. J Neurosci. 2002;22(3):991–1001.

529 35. Deussing JM, Breu J, Kühne C, Kallnik M, Bunck M, Glasl L, Yen YC, Schmidt MV,
530 Zurmühlen R, Vogl AM, Gailus-Durner V . Urocortin 3 modulates social
531 discrimination abilities via corticotropin-releasing hormone receptor type 2. J
532 Neurosci. 2010;30(27):9103–16.

533 36. Hegoburu C, Parrot S, Ferreira G, Mouly AM. Differential involvement of amygdala
534 and cortical NMDA receptors activation upon encoding in odor fear memory. Learn
535 Mem. 2014;21(12):651–5.

536 37. Liu J, Yu B, Neugebauer V, Grigoriadis DE, Rivier J, Vale WW, Shinnick-Gallagher
537 P, Gallagher JP . Corticotropin-releasing factor and Urocortin I modulate excitatory
538 glutamatergic synaptic transmission. J Neurosci. 2004;24(16):4020–9.

539 38. Autry AE, Wu Z, Kapoor V, Kohl J, Bambah-Mukku D, Rubinstein ND, Marin-
540 Rodriguez B, Carta I, Sedwick V, Tang M, Dulac C . Urocortin-3 neurons in the
541 mouse perifornical area promote infant-directed neglect and aggression. Elife.
542 2021;10.

543 39. Kuperman Y, Issler O, Regev L, Musseri I, Navon I, Neufeld-Cohen A, Gil S, Chen A

544 . Perifornical urocortin-3 mediates the link between stress-induced anxiety and energy
545 homeostasis. Proc Natl Acad Sci U S A. 2010;107(18):8393–8.

546 40. Yip SH, Liu X, Hessler S, Cheong I, Porteous R, Herbison AE. Indirect Suppression of
547 Pulsatile LH Secretion by CRH Neurons in the Female Mouse. Endocrinology.
548 2021;162(3).

549 41. Rivest S, Plotsky PM, Rivier C. CRF alters the infundibular LHRH secretory system
550 from the medial preoptic area of female rats: possible involvement of opioid receptors.
551 Neuroendocrinology. 1993;57(2):236–46.

552 42. Bagosi Z, Csabafi K, Karasz G, Jászberényi M, Földesi I, Siska A, Szabó G, Telegdy
553 G . The effects of the urocortins on the hypothalamic-pituitary-adrenal axis -
554 similarities and discordancies between rats and mice. Peptides. 2019;112:1–13.

555 43. Anthony TE, Dee N, Bernard A, Lerchner W, Heintz N, Anderson DJ. Control of
556 stress-induced persistent anxiety by an extra-amygdala septohypothalamic circuit.
557 Cell. 2014;156(3):522–36.

558 44. Li XF, Mitchell JC, Wood S, Coen CW, Lightman SL, O'Byrne KT . The effect of
559 oestradiol and progesterone on hypoglycaemic stress-induced suppression of pulsatile
560 luteinizing hormone release and on corticotropin-releasing hormone mRNA expression
561 in the rat. J Neuroendocrinol. 2003;15(5):468–76.

562 45. Zavala E, Voliotis M, Zerenner T, Tabak J, Walker JJ, Li XF, Terry JR, Lightman SL,
563 O'byrne K, Tsaneva-Atanasova K . Dynamic Hormone Control of Stress and Fertility.
564 Front Physiol. 2020;11:1457.

565 46. Kreisman MJ, McCosh RB, Tian K, Song CI, Breen KM. Estradiol Enables Chronic
566 Corticosterone to Inhibit Pulsatile Luteinizing Hormone Secretion and Suppress Kiss1
567 Neuronal Activation in Female Mice. Neuroendocrinology. 2020;110(6):501–16.

568 47. Dabrowska J, Hazra R, Guo JD, DeWitt S, Rainnie DG. Central CRF neurons are not
569 created equal: Phenotypic differences in CRF-containing neurons of the rat
570 paraventricular hypothalamus and the bed nucleus of the stria terminalis. Front
571 Neurosci. 2013;0(7 AUG):156.

572 48. Deussing JM, Chen A. The corticotropin-releasing factor family: Physiology of the
573 stress response. Vol. 98, Physiological Reviews. 2018. p. 2225–86.

574 49. Li XF, Bowe JE, Kinsey-Jones JS, Brain SD, Lightman SL, O'Byrne KT . Differential
575 role of corticotropin-releasing factor receptor types 1 and 2 in stress-induced
576 supression of pulsatile luteinising hormone secretion in the female rat. J
577 Neuroendocrinol. 2006;18(8):602–10.

578 50. Li XF, Bowe JE, Lightman SL, O'Byrne KT . Role of corticotropin-releasing factor
579 receptor-2 in stress-induced suppression of pulsatile luteinizing hormone secretion in
580 the rat. Endocrinology. 2005;146(1):318–22.

581 51. Raftogianni A, Roth LC, García-González D, Bus T, Kühne C, Monyer H, Spergel DJ,
582 Deussing JM, Grinevich V . Deciphering the Contributions of CRH Receptors in the
583 Brain and Pituitary to Stress-Induced Inhibition of the Reproductive Axis. Front Mol
584 Neurosci. 2018;11:305.

585 52. Kreisman MJ, McCosh RB, Breen KM . Role of CORT Duration and Estradiol
586 Dependence for Stress-level of CORT to Inhibit Pulsatile LH Secretion in Female
587 Mice. J Endocr Soc. 2021;Apr;5(Supplement_1):A552-.

588 53. Serge S, Rivier C. Influence of the paraventricular nucleus of the hypothalamus in the
589 alteration of neuroendocrine functions induced by intermittent footshock or
590 interleukin. Endocrinology. 1991;129(4):2049–58.

591 54. Wank I, Pliota P, Badurek S, Kraitsy K, Kaczanowska J, Griessner J, Kreitz S, Hess A,

592 Haubensak W . Central amygdala circuitry modulates nociceptive processing through
593 differential hierarchical interaction with affective network dynamics. Commun Biol.
594 2021;4(1):1–10.

595

596 **Figure 1.** Optogenetic stimulation of posterodorsal medial amygdala (MePD) urocortin-3
597 (Ucn3) neurons with blue light at 10 Hz, 10 mW suppressed pulsatile LH secretion in adult
598 ovariectomised (OVX) Ucn3-cre-tdTomato female mice. Infusion of bicuculline (BIC),
599 $GABA_A$ receptor antagonist, CGP, $GABA_B$ receptor antagonist, and AP5 and CNQX, NMDA
600 and AMPA receptor antagonists, respectively, into the posterodorsal medial amygdala (MePD)
601 during optogenetic stimulation of MePD urocortin-3 (Ucn3) neurons with blue light at 10 Hz,
602 10 mW completely blocked the suppressive effect of MePD Ucn3 neuronal activation on LH
603 pulsatility. Representative LH pulse profiles showing the effects of (A) control AAV-YFP
604 mice administered with aCSF receiving optical stimulation of 10 Hz, 10 mW, (B) AAV-ChR2
605 mice administered with aCSF receiving optical stimulation of 10 Hz, 10 mW, (C) Summary of
606 LH pulse interval for the pre-stimulation control period (1 h) and optical stimulation/infusion
607 period (1 h), (D) AAV-ChR2 mice administered with BIC, (E) AAV-ChR2 mice administered
608 with BIC receiving optical stimulation of 10 Hz, 10 mW, (F) Summary of LH pulse interval,
609 (G) AAV-ChR2 mice administered with CGP, (H) AAV-ChR2 mice administered with CGP
610 receiving optical stimulation of 10 Hz, 10 mW, (I) Summary of LH pulse interval, (J) AAV-
611 ChR2 mice administered with a combination of AP5 and CNQX, (K) AAV-ChR2 mice
612 administered with with a combination of AP5 and CNQX receiving optical stimulation of 10
613 Hz, 10 mW, (L) Summary of LH pulse interval. LH pulses detected by the DynePeak algorithm
614 are indicated with an asterisk located above each pulse on the representative LH pulse profiles.
615 For A-C +++$p<0.0001$ control period vs optic stimulation + aCSF (AAV-ChR2: n = 9);
616 ##$p<0.001$ optic stimulation vs control group (AAV-YFP: n = 3; no stimulation: n = 2). For

617 D-F n = 8-9 per group. For G-I n = 7 per group. For J-L n = 6 per group.

618 **Figure 2.** Optogenetic stimulation of posterodorsal medial amygdala (MePD) urocortin-3
619 (Ucn3) neuronal terminals in the hypothalamic paraventricular nucleus (PVN) with blue light
620 at 20 Hz, 15 mW elevated corticosterone (CORT) secretion in adult ovariectomised (OVX) +
621 E_2 Ucn3-cre-tdTomato female mice. CORT secretion time-course for mice receiving optical
622 stimulation initiated at 0 min and terminated at 60 min (1 h duration), followed by a 1 h
623 recovery period (60-120 min) for the AAV-ChR2 group (blue line, circles) and control group
624 (red line, squares). +$p<0.05$ AAV-ChR2 (n = 6) at time point 30 min and 60 min vs. control
625 (AAV-YFP: n = 3) at time point 30 min and 60 min.

626 **Figure 3.** Optogenetic stimulation of posterodorsal medial amygdala (MePD) urocortin-3
627 (Ucn3) neuronal terminals in the hypothalamic paraventricular nucleus (PVN) with blue light
628 at 20 Hz, 15 mW reduced LH pulsatility in adult ovariectomised (OVX) + E_2 Ucn3-cre-
629 tdTomato female mice. Representative LH pulse profiles showing the effects of (A) AAV-
630 YFP/WT mice receiving optical stimulation of 20 Hz, 5 mW, (B) AAV-ChR2 mice receiving
631 optical stimulation of 20 Hz, 5 mW, (C) Summary of LH pulse interval for the pre-stimulation
632 control period (1 h) and optic stimulation period (1 h). LH pulses detected by the DynePeak
633 algorithm are indicated with an asterisk located above each pulse on the representative LH
634 pulse profiles. +++$p<0.0001$ control period vs optic stimulation for AAV-ChR2 mice (n = 8);
635 ###$p<0.0001$ AAV-YFP/WT (AAV-YFP, n = 3; wild-type with AAV-ChR2, n = 2; no
636 stimulation, n = 2) vs AAV-ChR2 mice during optic stimulation.

637 **Figure 4.** Expression of AAV9-EF1a-double floxed-hChR2(H134R)-EYFP-WPRE-HGHpA
638 in posterodorsal medial amygdala (MePD) Urocortin-3 (Ucn3) neurons. (A-C) Representative
639 dual fluorescence photomicrographs of the MePD from a Ucn3-cre-tdTomato female OVX
640 mouse injected with AAV9-EF1a-double floxed-hChR2(H134R)-EYFP-WPRE-HGHpA.

641 Ucn3 neurons labelled with YFP (A) and tdTomato (B) appear yellow/orange (C). Scale bars
642 represent A, B, C, 20 μm.

643 **Figure 5.** Expression of AAV9-EF1a-double floxed-hChR2(H134R)-EYFP-WPRE-HGHpA
644 in Urocortin-3 (Ucn3) neuronal projection in the paraventricular nucleus of the hypothalamus
645 (PVN) originating from the posterodorsal medial amygdala (MePD). (A-Aii) Representative
646 dual fluorescence photomicrographs of the MePD from a Ucn3-cre-tdTomato female OVX +
647 E_2 mouse injected with AAV9-EF1a-double floxed-hChR2(H134R)-EYFP-WPRE-HGHpA.
648 Ucn3 neurons and projections labelled with (A) YFP and tdTomato merged, (Ai) higher power
649 view of YFP labelled MePD Ucn3 projections in the PVN and (Aii) higher power view of
650 tdTomato labelled MePD Ucn3 projections in the PVN. Scale bars represent A, 100 μm, Ai
651 and Aii, 10 μm. Blue box shows the YFP labelled MePD Ucn3 projections in the PVN, white
652 arrows point to YFP labelled MePD Ucn3 projections in the PVN and yellow arrow points to
653 optic cannula implantation site. 3V; third ventricle.

Figure 1

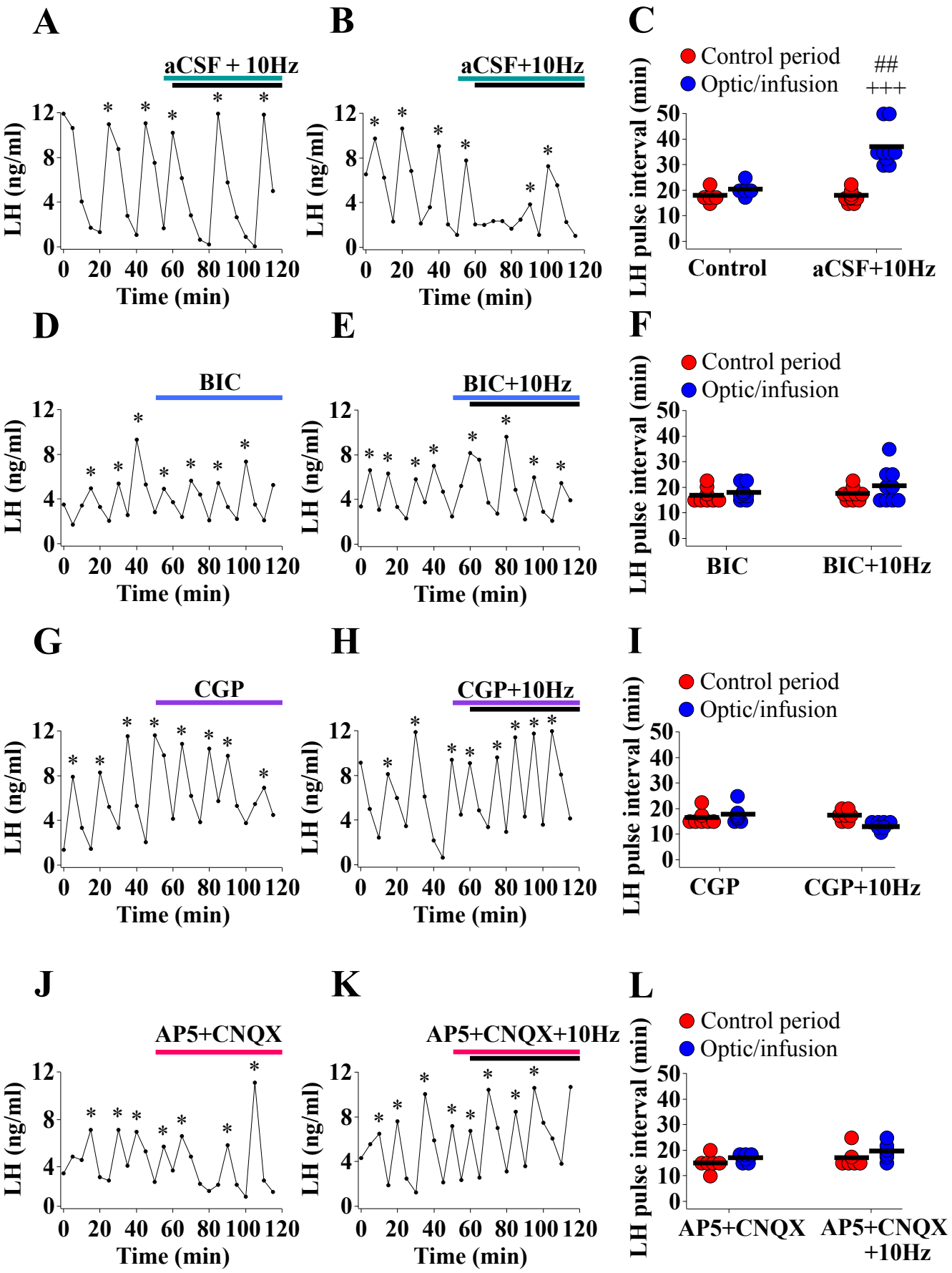
A
aCSF + 10Hz
LH (ng/ml)
Time (min)
B
aCSF+10Hz
LH (ng/ml)
Time (min)
C
Control period
Optic/infusion
##
+++
LH pulse interval (min)
Control
aCSF+10Hz
D
BIC
LH (ng/ml)
Time (min)
E
BIC+10Hz
LH (ng/ml)
Time (min)
F
Control period
Optic/infusion
LH pulse interval (min)
BIC
BIC+10Hz
G
CGP
LH (ng/ml)
Time (min)
H
CGP+10Hz
LH (ng/ml)
Time (min)
I
Control period
Optic/infusion
LH pulse interval (min)
CGP
CGP+10Hz
J
AP5+CNQX
LH (ng/ml)
Time (min)
K
AP5+CNQX+10Hz
LH (ng/ml)
Time (min)
L
Control period
Optic/infusion
LH pulse interval (min)
AP5+CNQX
AP5+CNQX
+10Hz

Figure 2

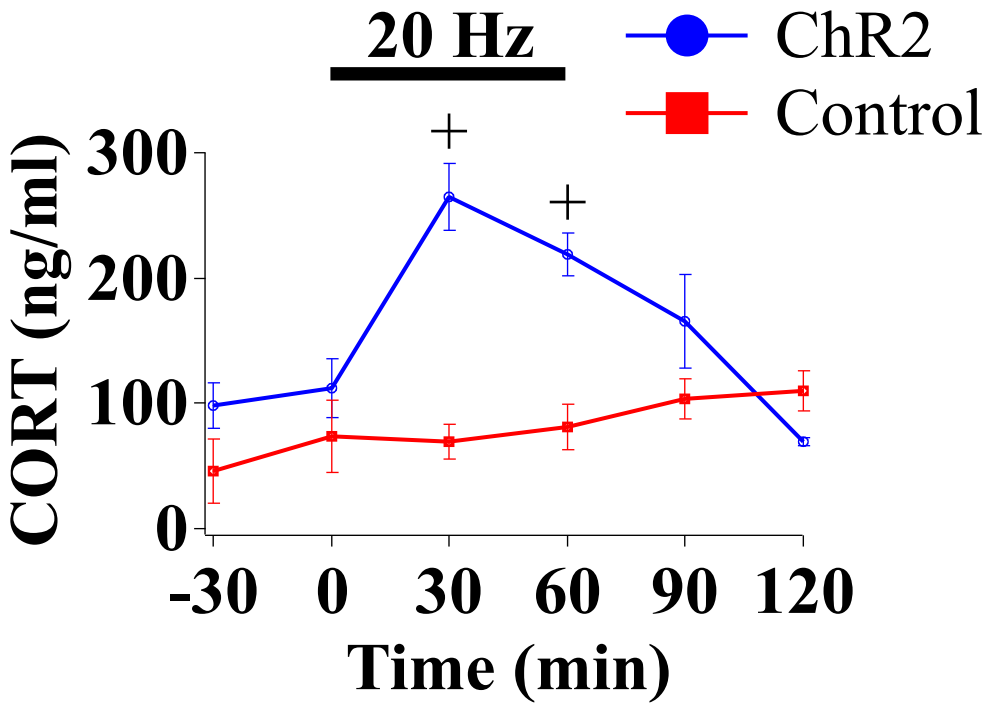
20 Hz
ChR2
Control
CORT (ng/ml)
300
200
100
0
-30
0
30
60
90
120
Time (min)

Figure 3

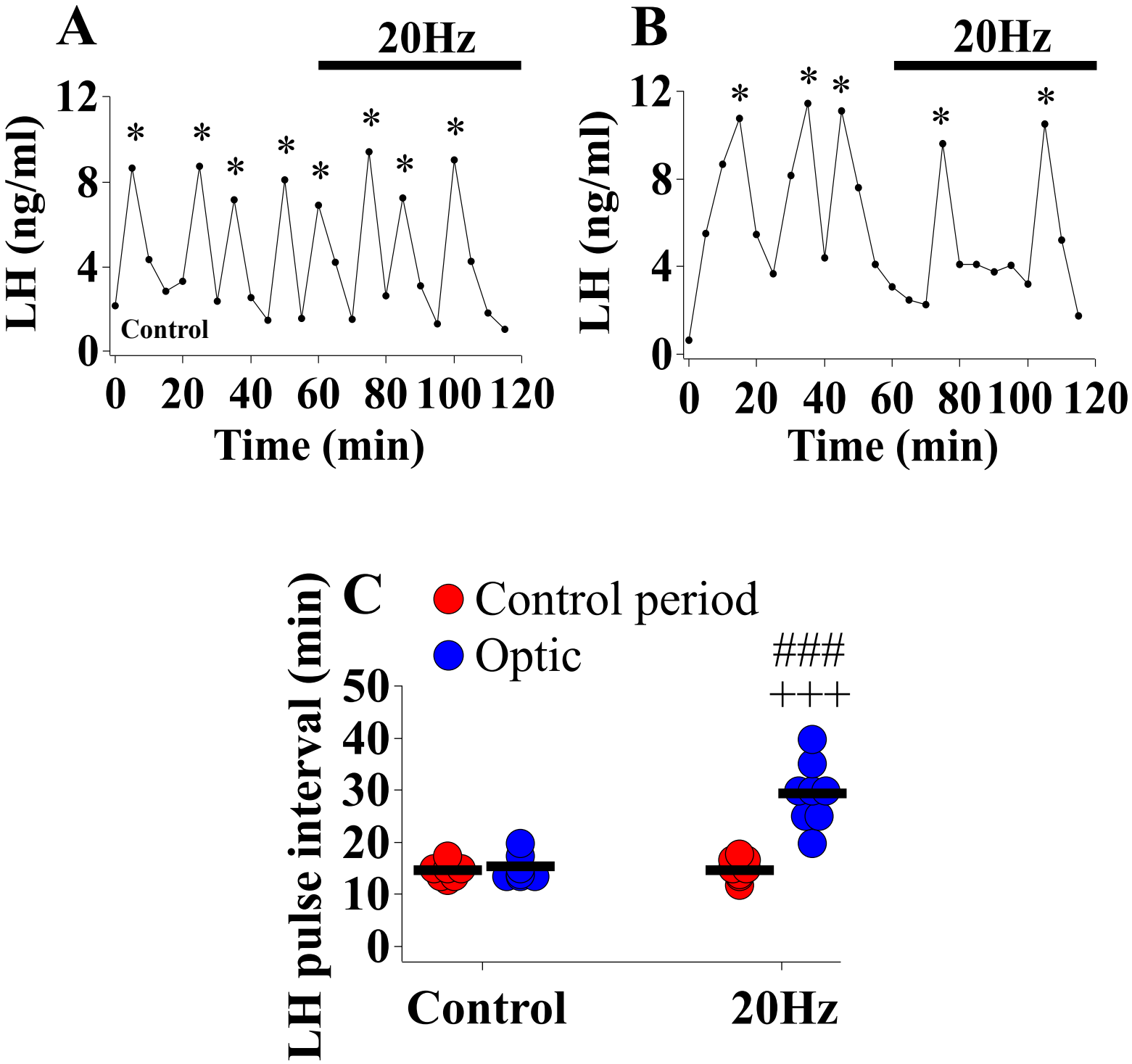
A
20Hz
LH (ng/ml)
12
8
4
0
Control
0 20 40 60 80 100 120
Time (min)
B
20Hz
LH (ng/ml)
12
8
4
0
0 20 40 60 80 100 120
Time (min)
C
Control period
Optic
###
+++
LH pulse interval (min)
50
40
30
20
10
0
Control
20Hz

Figure 4

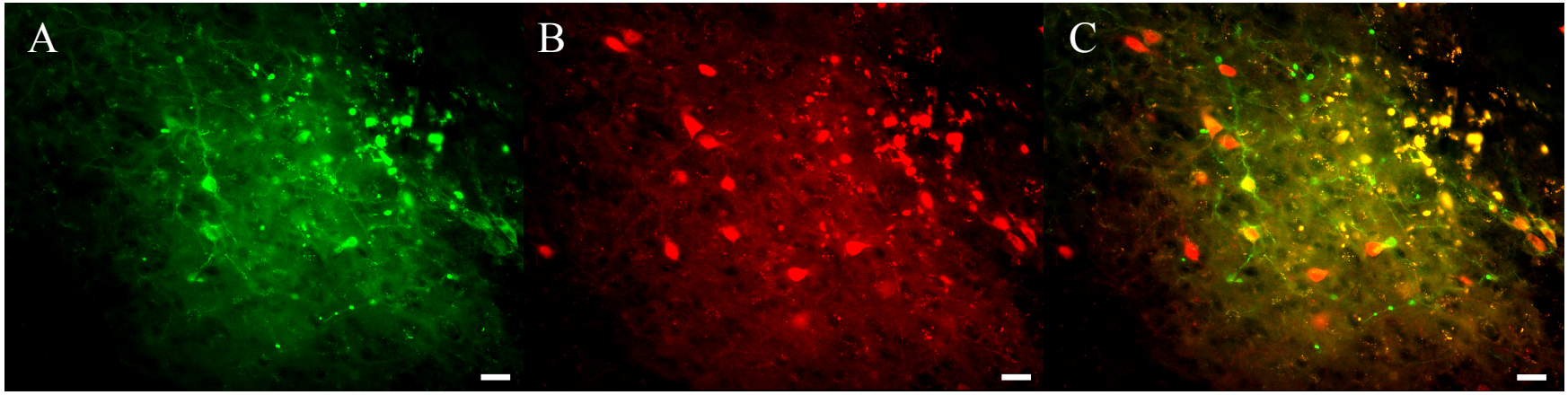
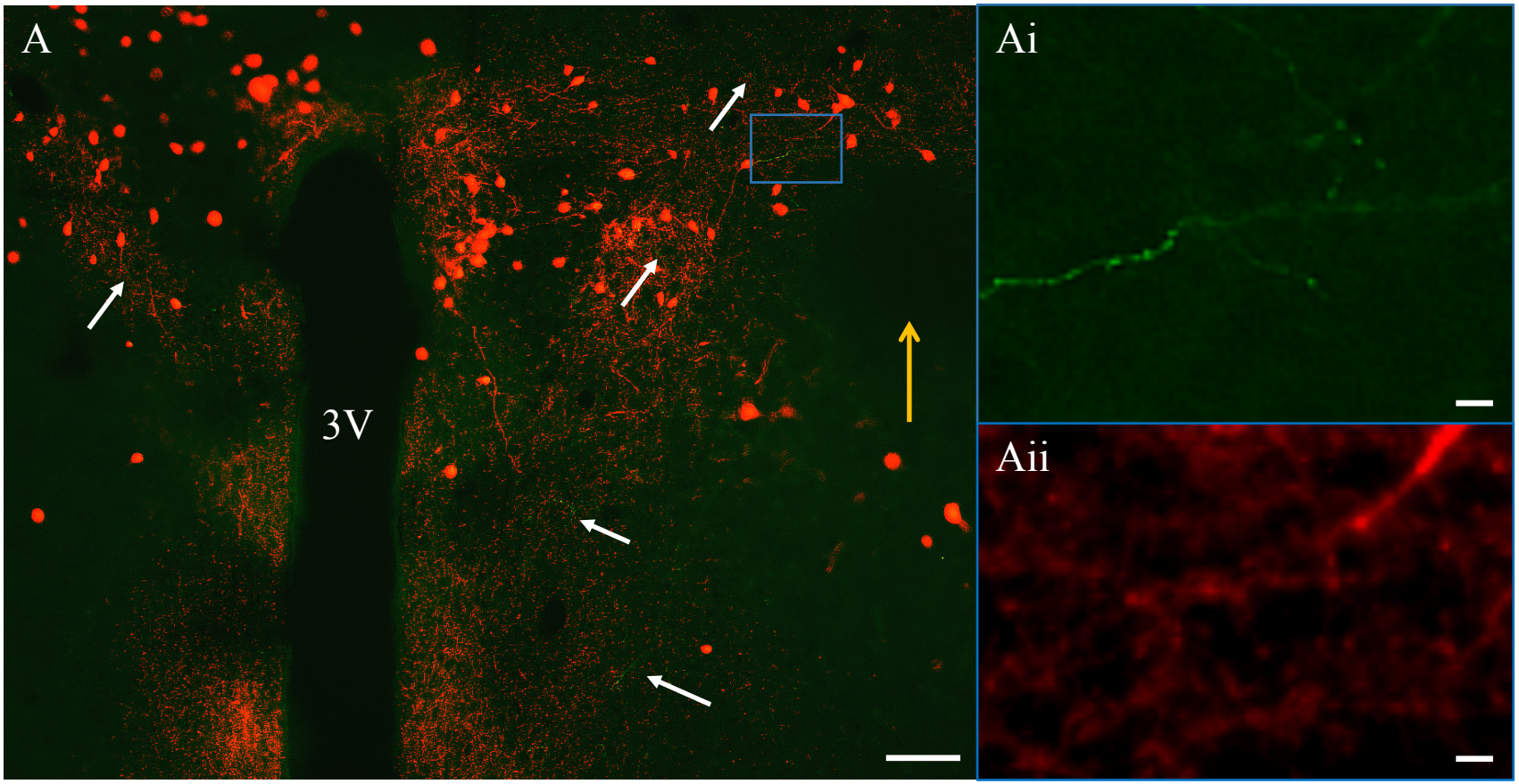
Figure 5